AIAA JOURNAL
Vol. 30, No. 11, November 1992

Emergence of Three-Dimensional Separation over a Suddenly Started Prolate Spheroid at Incidence

Tzuyin Wu* and Shan-Fu Shen†
Cornell University, Ithaca, New York 14853

By using a recently developed Eulerian program, the process toward three-dimensional separation is investigated through a numerical study of the laminar boundary layer over an impulsively started prolate spheroid. Details of the displacement-velocity distribution as well as the streamlines pattern near separation are examined and discussed. From the Lagrangian viewpoint, separation shows up, physically, as an abrupt eruption of a certain fluid packet that becomes deformed into one with zero thickness in the streamwise direction. In the present case the computed results suggest that this eruption, identified as a rapidly growing local thickness of boundary layer, first occurs at a point in the symmetry plane and then spreads in the crosswise direction. Figuratively, the boundary layer at separation would develop into a crescent-shaped mountain ridge thrusting itself into the main stream.The present findings are consistent with the features of incipient separation deduced from the Lagrangian analysis.

Nomenclature

e	= eccentricity of spheriod
h_1, h_2	= metric coefficients
p	= pressure
S	= transformed coordinate defined in Eq. (4)
t	= time
t/c	= axes ratio
U_e	= value of u at the edge of the boundary layer
u	= velocity component in the x direction
V_e	= value of v at the edge of the boundary layer
V_0, V_{90}	= constants in the velocity distribution at the edge of the boundary layer
v	= velocity component in the y direction
w	= velocity component in the z direction
x	= streamwise coordinate along the major axis of the prolate spheriod
y	= circumferential coordinate
z	= boundary-layer coordinate normal to the x and y directions
$\hat{\alpha}$	= angle of attack
α, β, γ	= computational coordinates
Δ	= indicates difference; also displacement thickness
δ	= difference operator in finite difference equations
μ	= average operator in finite difference equations
τ	= wall shear

Subscripts

w	= wall
x, y, z	= components in the x, y, and z directions, respectively
,	= derivatives

Superscripts

n	= nth time level in the finite difference equations
-	= quantities in the nose region
~	= quantities in the tail region

Presented as Paper 91-0544 at the AIAA 29th Aerospace Sciences Meeting, Reno, NV, Jan. 7-10, 1991; received Oct. 9, 1991; revision received May 6, 1992; accepted for publication May 7, 1992.

*Postdoctoral Fellow, Department of Mechanical Engineering; currently Associate Professor, Department of Mechanical Engineering, National Taiwan University, Taipei, Taiwan, ROC.

†John Edson Sweet Professor of Engineering, Department of Mechanical Engineering.

Introduction

WITH the fast growth of today's computing power, complete Navier-Stokes equations can now be solved numerically for moderate Reynolds number cases in a reasonable amount of computing time. On the other hand, many interesting yet perplexing problems associated with the high-Reynolds-number limit are still challenges to fluid mechanists. For instance, separation of the boundary layer under unsteady conditions has been controversial for quite some time. Recent studies and growing interest on this subject appear now to lead to some consensus. A prominent feature of unsteady separation is that it starts with an abrupt "eruption" of the boundary layer that ejects vorticity into the main stream. The classical and fundamental way of treating the separation problem is by means of the boundary-layer equations. From a practical viewpoint the sudden eruption is the manifestation of "singularity," a mathematical consequence resulting from the boundary-layer approximation that ignores any interaction. Many different studies[1-4] have established that the unsteady boundary-layer equations will turn singular in finite time.

The Lagrangian interpretation of unsteady separation, according to van Dommelen and Shen,[1,2] is that a certain fluid packet gets to be squeezed into one with zero thickness in the streamwise direction. For the two-dimensional case the extreme deformation of this packet would cause it to penetrate, together with the boundary-layer material on top of it, into the main stream and form a virtual barrier. In numerical computations of the boundary-layer equations, a conventional Eulerian scheme normally would not be able to give reliable answers close to the eruption time because of the singularity. In contrast, the Lagrangian criterion pinpoints the singularity and settles the controversy. However, the Lagrangian scheme, although advantageous in depicting separation, suffers, in actual computation, from the severe grid-distortion problem and the clumsy viscous terms. While with care, the unsteady Eulerian boundary-layer calculation could be made (e.g., in Wu and Shen[5]) to display the important characteristic growth near separation in the form of a "spike" similar to that from the Lagrangian result of Shen and Wu.[6]

The formation of the boundary-layer separation in a three-dimensional flow is still more complicated. The underlying mechanism of initiating separation through the singular deformation of a fluid packet, now augmented with another dimension, should, in principle, be unchanged. Earlier, a qualitative description of features of three-dimensional separation from a Lagrangian view was outlined by Shen,[7] and a thorough analysis has been recently presented by van Dommelen and Cow-

ley.[8] The latter deduced that the asymptotic structure of the singularity at separation is quasi-two-dimensional, with a rapidly rising displacement thickness in the form of a crescent-shaped ridge.

To study the details of the process that leads to separation on specific bodies and to attempt to control and influence the process, we have devised an Eulerian calculation that can diagnose the singularity without the inconveniences of the more precise Lagrangian simulation. Unlike most of the three-dimensional Eulerian codes, the present formulation is a time-accurate initial-value problem approach. Specification of a starting velocity profile needed to initiate the spatial integration in the conventional marching scheme is not required here; therefore, more general flows can be calculated. To cope with the inherent geometric singularity for three-dimensional bodies, we use a multizone technique. The boundary layer along the symmetry plane of a slender prolate spheroid undergoing an impulsive startup motion has been examined by Wu and Shen[5] as the first phase of a fully three-dimensional calculation. The spike signature in the displacement thickness was indeed captured. Several critical features in conjunction with the Lagrangian concept of separation were also discussed. The same problem was studied earlier by Xu and Wang.[9] However, confirmation of the singular features near separation was not part of their calculation.

In this paper, solutions over the entire surface of a prolate spheroid impulsively started from rest at both small and large incidences are presented. The steady-state version of the problem has been considered by many investigators.[10-19] In the steady case the limiting streamlines were traditionally used to define separation patterns in three-dimensional flows. Among the most notable consequences from these studies is perhaps the classification of closed- vs open-type separation suggested by Wang.[11-15] In his terminology convergence of the limiting streamlines defines the separation line on the surface. However, for the unsteady case it is now beyond dispute that separation starts off the wall. The skin friction and hence the wall streamlines have no direct significance, strictly speaking, in indicating separation. In the following, evolution of the limiting streamlines is also demonstrated, but the instantaneous pattern does not relate to separation that is diagnosed from a sudden eruption of boundary layer. Distributions of the displacement velocity in the tail region are also shown in detail, and the crescent structure at separation deduced asymptotically by van Dommelen and Cowley[8] is indeed confirmed. This development of a singular displacement velocity, key to the Lagrangian description of separation, was not provided by Ragab[20] in a previous calculation.

Governing Equations

Figure 1 illustrates the geometry and the boundary-layer coordinates of the prolate spheroid under consideration. In terms of this body-fitted coordinate system, the nondimensional forms of the boundary-layer equations are[17]

$$h_2\frac{\partial u}{\partial x}+h_1\frac{\partial v}{\partial y}+h_1h_2\frac{\partial w}{\partial z}+u\frac{\partial h_2}{\partial x}=0 \tag{1}$$

$$\frac{\partial u}{\partial t}+\frac{u}{h_1}\frac{\partial u}{\partial x}+\frac{v}{h_2}\frac{\partial u}{\partial y}+w\frac{\partial u}{\partial z}-\frac{vv}{h_1h_2}\frac{\partial h_2}{\partial x}=\frac{-1}{h_1}\frac{\partial p}{\partial x}+\frac{\partial^2 u}{\partial z^2} \tag{2}$$

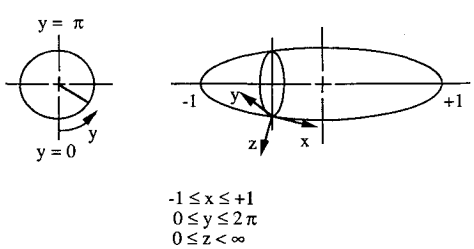

$-1 \le x \le +1$
$0 \le y \le 2\pi$
$0 \le z < \infty$

Fig. 1 Geometry and coordinate system.

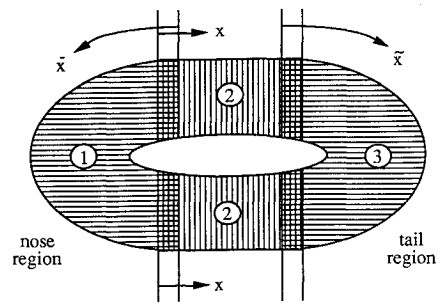

Fig. 2 Multiple zones.

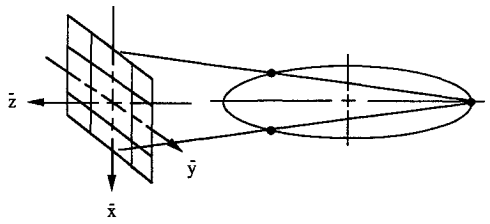

Fig. 3 Geometrical interpretation of the transformed coordinate system.

$$\frac{\partial v}{\partial t}+\frac{u}{h_1}\frac{\partial v}{\partial x}+\frac{v}{h_2}\frac{\partial v}{\partial y}+w\frac{\partial v}{\partial z}+\frac{uv}{h_1h_2}\frac{\partial h_2}{\partial x}=\frac{-1}{h_2}\frac{\partial p}{\partial y}+\frac{\partial^2 v}{\partial z^2} \tag{3}$$

where h_1 and h_2 are defined as

$$h_1=\sqrt{\frac{1-e^2x^2}{1-x^2}}, \qquad h_2=\sqrt{(1-e^2)(1-x^2)}$$

$$e=\sqrt{1-(t/c)^2}$$

Equations (1-3) have been properly scaled with the freestream velocity and the half-chord length of the prolate spheroid. The Reynolds number Re, as usual, was incorporated into the transverse coordinate z and velocity w. Based on the velocity profiles u and v, the skin friction and the displacement thickness are evaluated by

$$\tau_x=\left(\frac{\partial u}{\partial z}\right)_{z=0}, \qquad \tau_y=\left(\frac{\partial v}{\partial z}\right)_{z=0}$$

$$\Delta_x=\int_0^\infty\left(1-\frac{u}{U_e}\right)dz, \qquad \Delta_y=\int_0^\infty\left(1-\frac{v}{V_e}\right)dz$$

The velocities at the outer edge of the boundary layer approach the values specified by the potential flow[17]:

$$u=U_e=\frac{1}{(1-e^2x^2)^{1/2}}\left[V_0(1-x^2)^{1/2}\cos\hat{\alpha}+V_{90}\frac{t}{c}x\sin\hat{\alpha}\cos y\right]$$

and

$$v=V_e=V_{90}\sin\hat{\alpha}\sin y$$

as $z\to\infty$, where

$$V_0=\frac{e^2}{1-\dfrac{1-e^2}{2e}\ln\dfrac{1+e}{1-e}}, \qquad V_{90}=\frac{2V_0}{2V_0-1}$$

These velocities must then be brought to nil at the wall by viscous action. The pressure gradients $(-1/h_1)(\partial p/\partial x)$ and $(-1/h_2)(\partial p/\partial y)$ in the momentum equations (2) and (3) are

thus evaluated in terms of the freestream velocities U_e and V_e according to the inviscid Euler equations. The initial profiles needed to trigger the time integration after an impulsive startup are obtained from the Rayleigh solution.

When describing a closed object, a "geometric singularity" will be encountered if a single set of body-oriented coordinates is used.[21] In the present formulation, h_1 and h_2 become singular at both $x = -1$ and $x = 1$. Our remedy is to split the prolate spheroid into several regions (multizone approach) and apply a different coordinate system in both the nose and tail regions (Figs. 2 and 3). A transformation that removes this geometric singularity was proposed by Cebeci et al.[21] Define

$$\frac{d\bar{S}}{\bar{S}} = \frac{h_1\,dx}{h_2} = \frac{\sqrt{1-e^2x^2}\,dx}{\sqrt{1-e^2(1-x^2)}}$$

with $\bar{S} = 0$ at $x = -1$. It follows that

$$\bar{S} = B\exp\left[\frac{e}{\sqrt{1-e^2}}\sin^{-1}(ex) + A\right] \times \left[\frac{\sqrt{1-e^2}\sqrt{1-e^2x^2} - e^2x + 1}{\sqrt{1-e^2}\sqrt{1-e^2x^2} + e^2x + 1}\right]^{1/2}\sqrt{\frac{1+x}{1-x}} \tag{4}$$

where A and B are mapping constants. With transformation (4) and letting

$$\bar{x} = \bar{S}\cos y \qquad u = \bar{u}\cos y + \bar{v}\sin y$$
$$\bar{y} = \bar{S}\sin y \qquad v = -\bar{u}\sin y + \bar{v}\cos y \tag{5}$$
$$\bar{z} = z \qquad w = \bar{w}$$

Equations (1-3) then become

$$\frac{1}{\bar{h}}\left(\frac{\partial\bar{u}}{\partial\bar{x}} + \frac{\partial\bar{v}}{\partial\bar{y}}\right) + \frac{\partial\bar{w}}{\partial\bar{z}} - \bar{R}(\bar{x}\bar{u} + \bar{y}\bar{v}) = 0 \tag{6}$$

$$\frac{\partial\bar{u}}{\partial t} + \frac{\bar{u}}{\bar{h}}\frac{\partial\bar{u}}{\partial\bar{x}} + \frac{\bar{v}}{\bar{h}}\frac{\partial\bar{u}}{\partial\bar{y}} + \bar{w}\frac{\partial\bar{u}}{\partial\bar{z}} + \bar{R}\bar{v}(\bar{x}\bar{v} - \bar{y}\bar{u}) = \frac{-1}{\bar{h}}\frac{\partial p}{\partial\bar{x}} + \frac{\partial^2\bar{u}}{\partial\bar{z}^2} \tag{7}$$

$$\frac{\partial\bar{v}}{\partial t} + \frac{\bar{u}}{\bar{h}}\frac{\partial\bar{v}}{\partial\bar{x}} + \frac{\bar{v}}{\bar{h}}\frac{\partial\bar{v}}{\partial\bar{y}} + \bar{w}\frac{\partial\bar{v}}{\partial\bar{z}} - \bar{R}\bar{u}(\bar{x}\bar{v} - \bar{y}\bar{u}) = \frac{-1}{\bar{h}}\frac{\partial p}{\partial\bar{y}} + \frac{\partial^2\bar{v}}{\partial\bar{z}^2} \tag{8}$$

where

$$\bar{h} = \frac{h_2}{\bar{S}}, \qquad \bar{R} = \frac{1}{\bar{S}}\left(\frac{1}{h_2} - \frac{1}{h_1h_2}\frac{\partial h_2}{\partial x}\right)$$

Geometrically, Eqs. (4) and (5) may be interpreted as projecting the nose part of the prolate spheroid onto a vertical plane, and a set of Cartesian grids $(\bar{x}, \bar{y})$ is then drawn on that plane (Fig. 3). In the limiting case, a sphere ($e = 0$), the transformation procedure reduces to exactly a stereograph projection. The same treatment is applied to the rear end $x = +1$.

Numerical Method

The numerical procedures closely follow those given by Wu and Shen,[5] with only a minor modification to cope with the extra direction introduced here. For completeness, a brief description of the solution scheme is stated as follows.

In the present multizone scheme the solution domain is decomposed into three regions, as shown in Fig. 2, in such a way that adjacent regions overlap with each other. Geometric singularities are properly removed by applying the transformed coordinates system described in the last section to the nose and tail regions. Each physical region (x, y, z) is mapped to a unit box (α, γ, β) by using appropriate mapping functions (see, e.g., Wu.[22]). The governing equations in these computational coordinates are then discretized. Calculations are performed separately in different regions, and the required boundary conditions on the interface of a specific region are obtained from interpolating the interior solution of the neighboring region. The strategy has been proven to be successful in the previous symmetry-plane calculation. Detailed results can be found in Ref. 22.

Unlike the conventional space-marching technique, we formulate strictly an initial-value problem in which integration of the boundary-layer equations marches in the timewise direction only. At each time step, a central difference is used to discretize the diffusion terms, whereas a flow-dependent, second-order upwind differencing scheme is applied to the convection terms in accordance with their hyperbolic nature. Thus, the domain of dependence rule[16,23] is satisfied. In treating the nonlinear terms, a noniterative predictor-corrector formulation of Douglas and Jones[24] is adopted. That is, between two successive time steps n and $n + 1$, predicted values are first evaluated at $n + \frac{1}{2}$ by a first-order scheme, and all of the nonlinear coefficients in the subsequent correction step are then replaced by these predicted quantities. In both predictor and corrector steps the governing equations are decoupled and hence can be solved independently. A fully implicit scheme is preferred in solving the predictor values for stability consideration. Second-order accuracy in temporal difference can be restored by following a Crank-Nicolson-like corrector step.

Applying the preceding discretization procedures to the momentum equations (2) and (3), the resulting finite difference equations for the corrector step are, in the computational space (α, γ, β),

$$\left\{1 + \frac{\Delta t\alpha_{,x}u}{2h_1\Delta\alpha}\delta_\alpha^{\pm} + \frac{\Delta t\gamma_{,y}v}{2h_2\Delta\gamma}\delta_\gamma^{\pm} - \frac{\Delta t\beta_{,z}^2}{2\Delta\beta^2}\delta_\beta^2 - \frac{\Delta t(\beta_{,zz} - \beta_{,t} - \beta_{,z}w)}{4\Delta\beta}(2\mu\delta)_\beta\right\}^{n+1/2}\Delta u^{n+1}$$
$$= \frac{-\Delta t}{h_1}\frac{\partial p}{\partial x} + \frac{\Delta t v^{n+1/2}v^{n+1/2}}{h_1h_2}\frac{\partial h_2}{\partial x} + \Delta t\left\{-\frac{\alpha_{,x}u}{h_1\Delta\alpha}\delta_\alpha^{\pm} - \frac{\gamma_{,y}v}{h_2\Delta\gamma}\delta_\gamma^{\pm} + \frac{\beta_{,z}^2}{\Delta\beta^2}\delta_\beta^2 + \frac{(\beta_{,zz} - \beta_{,t} - \beta_{,z}w)}{2\Delta\beta}(2\mu\delta)_\beta\right\}^{n+1/2}u^n \tag{9}$$

$$\left\{1 + \frac{\Delta t\alpha_{,x}u}{2h_1\Delta\alpha}\delta_\alpha^{\pm} + \frac{\Delta t\gamma_{,y}v}{2h_2\Delta\gamma}\delta_\gamma^{\pm} - \frac{\Delta t\beta_{,z}^2}{2\Delta\beta^2}\delta_\beta^2 - \frac{\Delta t(\beta_{,zz} - \beta_{,t} - \beta_{,z}w)}{4\Delta\beta}(2\mu\delta)_\beta\right\}^{n+1/2}\Delta v^{n+1}$$
$$= \frac{-\Delta t}{h_2}\frac{\partial p}{\partial y} - \frac{\Delta t u^{n+1/2}v^{n+1/2}}{h_1h_2}\frac{\partial h_2}{\partial x} + \Delta t\left\{-\frac{\alpha_{,x}u}{h_1\Delta\alpha}\delta_\alpha^{\pm} - \frac{\gamma_{,y}v}{h_2\Delta\gamma}\delta_\gamma^{\pm} + \frac{\beta_{,z}^2}{\Delta\beta^2}\delta_\beta^2 + \frac{(\beta_{,zz} - \beta_{,t} - \beta_{,z}w)}{2\Delta\beta}(2\mu\delta)_\beta\right\}^{n+1/2}v^n \tag{10}$$

where

$$\Delta u^{n+1} = u^{n+1} - u^n$$
$$\Delta v^{n+1} = v^{n+1} - v^n$$

and $\alpha_{,x}$, $\gamma_{,y}$, $\beta_{,t}$, $\beta_{,z}$, and $\beta_{,zz}$ denote the derivatives of the corresponding mapping functions. The difference operators used are defined as follows:

$$\delta = (\cdot)_{i+1/2} - (\cdot)_{i-1/2}, \qquad \delta^2 = (\cdot)_{i+1/2} - 2(\cdot)_i + (\cdot)_{i-1}$$
$$u = \tfrac{1}{2}[(\cdot)_{i+1/2} + (\cdot)_{i-1/2}]$$

$$\delta^+ = \tfrac{1}{2}[3(\cdot)_i - 4(\cdot)_{i-1} + (\cdot)_{i-2}]$$

$$\delta^- = \tfrac{1}{2}[-3(\cdot)_i + 4(\cdot)_{i+1} - (\cdot)_{i+2}]$$

For direct solving of the preceding finite difference equations, one will need to invert a large matrix with blocklike entries. To cut down the computational work, Eqs. (9) and (10) are factored into three sweeps according to the approximate factorization procedure of Warming and Beam.[25] Each sweep now involves solving a relatively smaller system of algebraic equations with a scalar tridiagonal or pentadiagonal coefficient matrix only:

$$\left\{1 - \frac{\Delta t \beta_{,z}^2}{2\Delta\beta^2}\delta_\beta^2 - \frac{\Delta t(\beta_{,zz} - \beta_{,t} - \beta_{,z}w)}{4\Delta\beta}(2\mu\delta)_\beta\right\}^{n+\frac{1}{2}} \Delta u''^{n+1}$$

$$= \text{RHS of Eq. (9)}$$

$$\left\{1 + \frac{\Delta t \gamma_{,y} v}{2h_2\Delta\gamma}\delta_\gamma^{\pm}\right\}^{n+\frac{1}{2}} \Delta u'^{n+1} = \Delta u''^{n+1}$$

$$\left\{1 + \frac{\Delta t \alpha_{,x} u}{2h_1\Delta\alpha}\delta_\alpha^{\pm}\right\}^{n+\frac{1}{2}} \Delta u^{n+1} = \Delta u'^{n+1}$$

Both matrices can be easily inverted by efficient tridiagonal and pentadiagonal solvers. With u and v obtained, the normal velocity w is then updated from integrating the continuity equation (1) by Simpson's rule.

Similar numerical procedure are used to discretize the transformed equations in the nose and tail regions. Their final forms are omitted here.

Results and Discussion

Calculations were carried out for a prolate spheroid of axes ratio ¼ at both small (6 deg) and large (50 deg) incidences. Because of the symmetry property, only half of the body was considered. Prior to the full-scale computation, the accuracy of the numerical scheme, assessed from a grid refinement strategy, was investigated. In the final production runs, typical mesh sizes used in the calculations were $50 \times 25 \times 121$ for the nose region, $61 \times 81 \times 121$ in the main body, and $100 \times 50 \times 121$ for the tail region. Numerals associated with the grid refer to the number of grid points in the x, y, and z directions, respectively. All of the numerical computations were performed on Cornell's IBM 3090-600J supercomputer under vector mode. Normally, the required CPU time for advancing one time step (double-precision arithmetic) was ~ 0.1 μs per grid point for most of the cases. The next section provides a brief discussion on the numerical accuracy. Then computed results at two different incidences, $\hat{\alpha} = 6$ and 50 deg, are given. Emphasis will be placed on the initiation of separation evidenced by the emergence of a Lagrangian singularity in the flow.

Test of Accuracy

The zero-degree incidence case is calculated here as a bench test of the present numerical scheme. The accuracy of the calculation is evaluated by examining the effect of grid refinement on the value of wall shear at the front stagnation point. The steady solution of the three-dimensional stagnation flow has been obtained by Howarth[26] in terms of a power series expansion. In the present formulation the derivative of the wall shear at the forward stagnation point is calculated by

$$\bar{\tau}_0 = (\bar{\tau}_{\bar{x},\bar{x}}/\bar{h})/(\bar{U}_{e,\bar{x}}/\bar{h})^{3/2}$$

where the term $(\bar{U}_{e,\bar{x}}/\bar{h})^{3/2}$ is incorporated as a scaling factor so that the steady-state value of $\bar{\tau}_0$ is equivalent to the $f''(0)$ defined by Howarth.[26] For the axisymmetric case, $f''(0) = 1.312$.

Figure 4 shows the temporal evolution of $\bar{\tau}_0$. It is observed that shortly after the impulsive startup the wall shear at the front stagnation point quickly reaches a steady value. Table 1 lists the values of $\bar{\tau}_0$ at $t = 0.2$ calculated at three successively finer meshes with time step Δt ranging equally from 0.02 to 0.005. All three results appear to be quite close to the steady-state value of 1.312 obtained by Howarth.[26] Using the Richardson extrapolation procedure (RE), the last row of the table contains the extrapolated value of $\bar{\tau}_0$ from the aforementioned three different meshes. Taking this value as an exact solution, errors in $\bar{\tau}_0$ associated with each grid size are listed in the last column. Quadratic convergency is evident. Although linearized von Neumann stability analysis predicts that the three-dimensional version of the approximate factorization scheme is only conditionally stable, in the present predictor-corrector formulation, no instability was encountered when the calculations were performed on the three preceding meshes.

At $\hat{\alpha} = 0$ deg, every meridian plane that cuts through the prolate spheroid is necessarily a symmetry plane in this special case. The separation history of the boundary layer on the symmetry plane has been described in Ref. 5. No further results will be given here.

Displacement Velocity

In the previous symmetry plane results,[5] separation was diagnosed from the occurrence of a "spike signature" in the distribution of streamwise displacement thickness. In a three-dimensional flow neither of the displacement thicknesses Δ_x and Δ_y, which are defined in terms of the two velocity components u and v, truly represents the effective thickening of the body due to the boundary layer.[27] However, it is this thickening action of the boundary layer that drives the perturbation to the outer flow and changes it significantly as separation is approached. To perceive the separation process, we thus choose to look in the tail region at the evolution of the displacement velocity $\tilde{w}_w$ at the outer edge of the boundary layer.

The displacement velocity, in terms of our present transformed coordinates, has the following form:

$$\tilde{w}_w = \frac{1}{\tilde{h}}\frac{\partial}{\partial\tilde{x}}(\tilde{U}_e\tilde{\Delta}_{\tilde{x}}) + \frac{1}{\tilde{h}}\frac{\partial}{\partial\tilde{y}}(\tilde{V}_e\tilde{\Delta}_{\tilde{y}}) - \tilde{R}\tilde{x}(\tilde{U}_e\tilde{\Delta}_{\tilde{x}}) - \tilde{R}\tilde{y}(\tilde{V}_e\tilde{\Delta}_{\tilde{y}}) \quad (11)$$

By definition, the displacement velocity measures the difference between viscous transverse velocity and its inviscid counterpart at the outer edge of the boundary layer. In the concept of matched asymptotic expansions, it then describes how the inner viscous layer is matched with the outer inviscid flow. Asymptotically, this term should remain on the order of one

Table 1 Effects of grid refinement on the value of skin friction at the stagnation point

Grid size	$\bar{\tau}_0$	Error
$30 \times 15 \times 31$	1.305591	0.006341
$60 \times 30 \times 61$	1.310520	0.001412
$120 \times 60 \times 121$	1.311590	0.000342
RE	1.311932	—

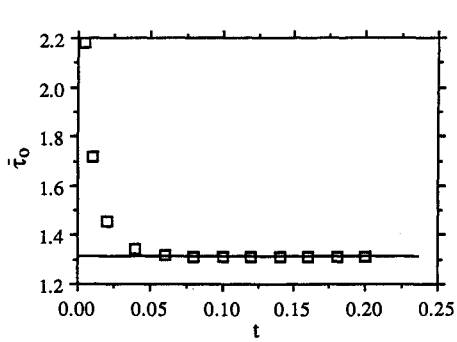

Fig. 4 Temporal evolution of $\bar{\tau}_0$ (grid size $120 \times 60 \times 121$), —— steady-state value of Howarth.

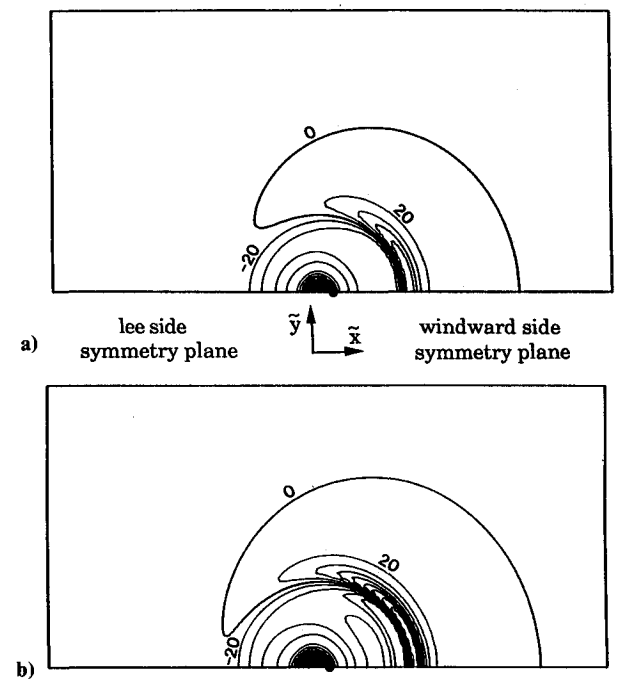

Fig. 5 Distribution of the displacement velocity in the tail region ($\hat{\alpha} = 6$ deg): a) $t = 0.17$; b) $t = 0.19$.

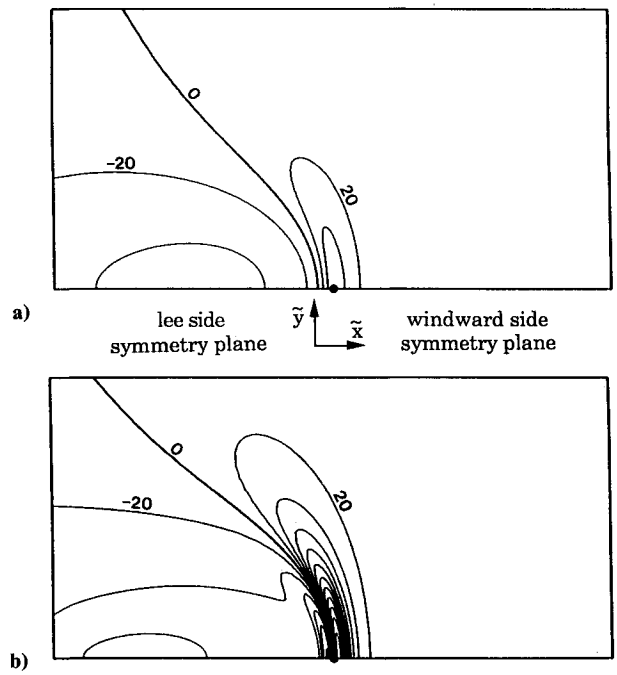

Fig. 6 Distribution of the displacement velocity in the tail region ($\hat{\alpha} = 50$ deg): a) $t = 0.09$; b) $t = 0.11$.

for the boundary layer assumption to be valid. The significance of this term is also found in the classical viscous-inviscid interaction theory, since it reflects the displacing effect of the viscous action through which the boundary layer would interact with the outer main stream.

Figure 5 shows the contour plots of the distribution of displacement velocity $\tilde{w}_w$ in the tail region for the 6-deg incidence case. In the axisymmetric case these contour lines would necessarily appear as concentric circles centered at the rear end point when looking toward the prolate spheroid along the axial direction. Because of the presence of a small angle of attack, the symmetry is destroyed. Strong displacement velocity is found to evolve first at the windward symmetry plane and then curve toward the leeside of the symmetry plane in the form of a crescent-shaped ridge. As a consequence of this strong blowing effect, the boundary-layer material constructs a closed front normal to the direction of the local streamlines, much like a virtual barrier, obviously impenetrable to the oncoming flow inside the boundary layer. The flow must then eject itself vertically into the freestream.

The distribution of the displacement velocity in the tail region for the 50-deg incidence case is given in Fig. 6. As in the preceding case, at $t = 0.11$, it is seen that close to the rear end of the spheroid contours of the displacement velocity rapidly evolve into an elongated kidney-shaped mountain ridge, with a sharp gradient in the streamwise direction while descending away from the symmetry plane in a somewhat milder manner. Establishment of these striplike contours substantiates the result of the asymptotic analysis of van Dommelen and Cowley[8] that the structure of singularity just prior to separation is quasi-two-dimensional, with a streamwise length scale much shorter than that in the crosswise direction. In fact, the appearance of contours of boundary-layer thickness conjectured by van Dommelen and Cowley (Fig. 2c in Ref. 8) is very similar to what we have obtained in the displacement-velocity distribution here (Fig. 6b).

The singular behavior of the boundary layer is more convincingly demonstrated in Fig. 7, where the distributions of $\tilde{w}_w$ at $t = 0.09$ and 0.11 are displayed in three-dimensional surface plots. It is observed that, beginning at $t = 0.09$, a hump is

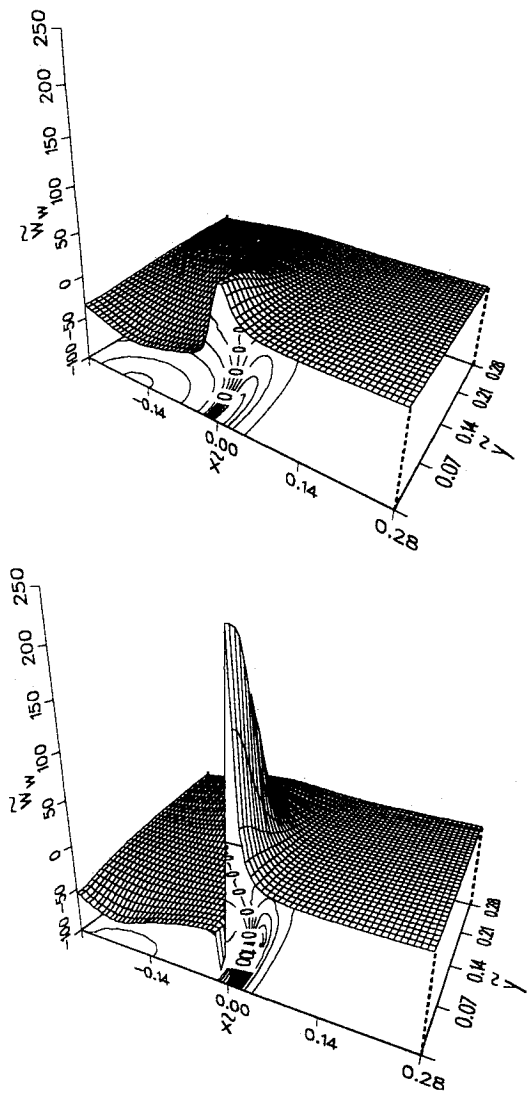

Fig. 7 Perspective view of the distribution of the displacement velocity in the tail region ($\hat{\alpha} = 50$ deg): a) $t = 0.09$; b) $t = 0.11$.

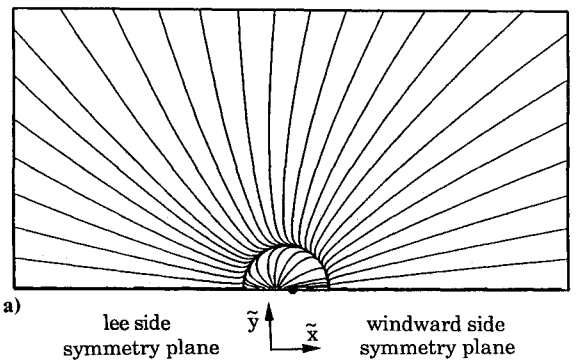

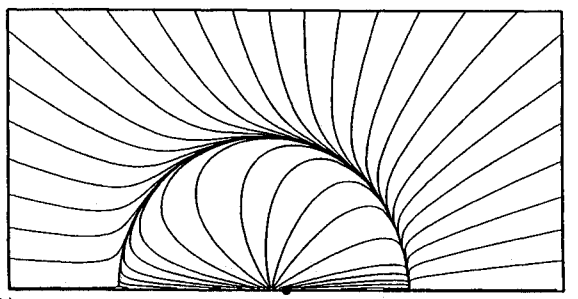

Fig. 8 Limiting streamlines in the tail region ($\hat{\alpha} = 6$ deg): a) $t = 0.05$; b) $t = 0.19$.

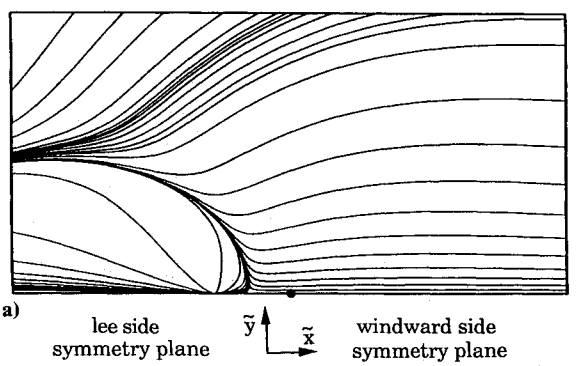

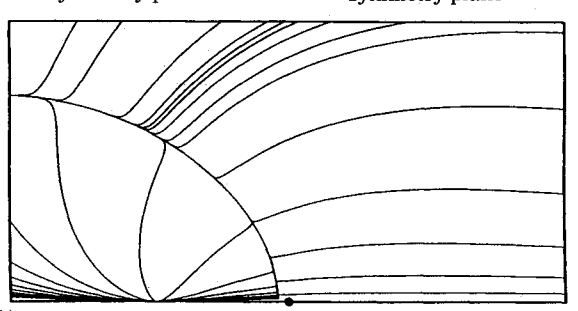

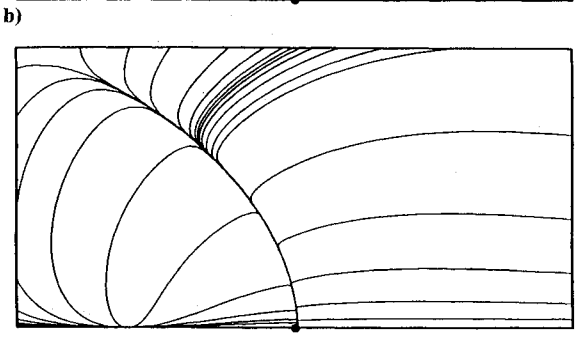

Fig. 9 Limiting streamlines in the tail region ($\hat{\alpha} = 50$ deg): a) $t = 0.04$; b) $t = 0.05$; c) $t = 0.06$.

formed near the rear vertex. Strong vertical ejection in $\tilde{w}_w$ occurs between $t = 0.09$ and 0.11, clearly incongruous with the order one assumption made in the boundary-layer approximation. The emergence of separation is then evidenced as a sudden burst of the boundary-layer flow into a narrow plume penetrating into the main stream.

In Fig. 5 it can be seen that a deep well of negative displacement velocity appears in the vicinity of the rear stagnation point. A large negative value of $\tilde{w}_w$ indicates a strong suction effect due to the reversal of the flow along the rear stagnation line. A similar phenomenon is also present in the two-dimensional case. Its existence seems to have been overlooked before.

Limiting Streamlines

In the past the limiting streamlines have been extensively used in defining and classifying separation in three-dimensional flows. From the Lagrangian descriptions of Shen[7] and van Dommelen and Cowley,[8] separation is depicted as formation of a "front" by the particle paths due to the singular contraction of a fluid element along its trajectory. For the steady problem involving a fixed wall, limiting streamlines coincide with the particle paths. Convergence of limiting streamlines should have an important consequence in identifying steady separation.[7] In an unsteady flow, separation generally results from the motion of particles away from the wall. The limiting streamlines, which describe the flow development only close to the surface, do not seem to provide critical information that can be strictly correlated to the evolving unsteady separation off the wall.

Evolution of the limiting streamlines in the tail region is shown in Fig. 8 for $\hat{\alpha} = 6$ deg. Shortly after the spheroid is set into motion, a closed bubble containing recirculating flow is formed in the tail region. Because of the slight asymmetry, the limiting streamline enclosing the reversed flow region is seen to emanate from the leeside symmetry plane and then circle back to merge into the symmetry plane again at the windward side. This is obviously what was originally described by Lighthill[28] as a classical example of "steady separation," in which streamlines leave the surface along the two separatrices of a saddle point that, after embracing the body, merge into a nodal point. It has also been classified as a "type I separation" in the topological study of steady limiting streamline patterns due to Chapman.[29] The size of this recirculation region increases with time, but the bubble remains closed (Figs. 8a and 8b). However, according to the steady-state calculation of Cebeci and Su,[30] the bubble will eventually open from the leeside and the merging of limiting streamlines will then change, in the terminology of Wang,[11-15] to an open type.

The limiting streamline pattern for $\hat{\alpha} = 50$ deg appears to be somewhat more complicated than that for the 6-deg incidence case. Starting from $t = 0.04$, a closed recirculation region of the instantaneous streamlines is formed (Fig. 9). The limiting streamline forming the boundary of the bubble emerges from the symmetry plane at a point near the end of the spheroid and turns back to intersect the symmetry plane again at a point on leeside (at the far left corner of Fig. 9, outside the tail region). The bubble is open from the leeward symmetry plane at $t = 0.06$ (Fig. 9c), and the pattern of limiting streamlines changes from closed to open type and stays open thereafter. It is also found that the limiting streamlines near the rear end now merge toward the symmetry plane instead of away from it as previously noted. Note that these open and closed patterns occur while the boundary layer is behaving normally, and is therefore unseparated.

Limiting streamlines in the main body region are shown in Fig. 10. In these plots the surface of the prolate spheroid is unwrapped into a rectangular sheet. The rear stagnation point is located near the upper right corner of the domain where part of the aforementioned recirculating flow is observed in Fig. 10a. At small time, most of the limiting streamlines in the main region run from the windward symmetry plane to the

leeside symmetry plane. The opening of the recirculation region from the leeside symmetry plane is clearly seen at $t = 0.06$ in Fig. 10a. At the same time, the reversal of the crossflow near the leeside symmetry plane is also observed to gradually extend toward the upstream direction. At approximately $t = 0.08$, another region of circumferentially reversed flow is formed near the front end of the leeward symmetry plane (Fig. 10b). In contrast to the one near the rear stagnation point, this region grows rapidly downstream. As a result, a second open-type convergence of limiting streamlines evolves at the front. In Fig. 10c the two areas where limiting streamlines merge together are seen to connect with each other at $t = 0.11$, by which time almost all of the limiting streamlines near the entire leeward symmetry plane have reversed their directions (i.e., are flowing away from the symmetry plane).

The appearance of these closed or open types of limiting streamline patterns is apparently the consequence of flow reversals in the streamwise and circumferential directions. However, these interesting features emerge while the boundary layer is yet to develop any evidence of anomalous behavior. A drastic local thickening of the boundary layer was not found, at least before $t = 0.11$. The notion of relating the emergence of a specific limiting streamline pattern to the onset of unsteady separation is thus untenable.

Instantaneous Streamlines

Although the role of limiting streamlines over the body surface may be inconclusive, the critical features of unsteady separation can be seen from the developing streamline pattern "away" from the wall. In Fig. 11 the instantaneous distributions of streamlines in the symmetry plane ($\tilde{y} = 0$) of the tail region are shown at $t = 0.19$ and 0.21 for $\hat{\alpha} = 6$ deg. The streamlines are generated by marching in the symmetry plane along a path tangent to the projection of local velocity:

$$\frac{d\tilde{z}}{d\tilde{x}} = \frac{\tilde{w}}{\tilde{u}}$$

Two familiar vortices are observed to evolve near the rear stagnation point, in a slightly asymmetrical pattern because of the small angle of attack. At $t = 0.19$, the vortex at leeside remains regular, whereas near the vortex at the windward side the streamlines develop a spike signature similar to that previously found in the displacement thickness, indicating that separation first occurs from the windward symmetry plane. The formation of this spike structure is clearly associated with the singular deformation of the nearby fluid elements. Of course, in unsteady flows, streamlines do not coincide with particle paths; thus, we do not actually "see" the fluid elements from the distribution of instantaneous streamlines. Nevertheless, large values of the local transverse velocity $\tilde{w}$ resulting from the severe contraction of fluid elements in the streamwise direction are manifested by an extreme clustering of the streamlines in a narrow spikelike region.

Figure 12 presents the instantaneous streamlines in the symmetry plane for the 50-deg incidence case. In this plot the freestream is flowing from right to left. Again, at $t = 0.11$, it is observed that, just inside the boundary of the vortex, a spike structure is established. A strong eruption of the boundary-layer flow is evident as this peaking phenomenon in the streamlines distribution becomes more pronounced at $t = 0.12$. The resulting flow pictures exhibited here are indeed consistent with the Lagrangian description of the separation process.

Singularity

According to the Lagrangian analysis of van Dommelen and Cowley,[8] the asymptotic structure of the singularity at separation in the present three-dimensional problem is one in which, close to the separation time t_s, the transverse displacement $\tilde{z}$ of a certain fluid particle blows up as $(t_s - t)^{-1/4}$ within a relatively thin strip of scales $|\tilde{x}_s - \tilde{x}| \sim (t_s - t)^{3/2}$, $|\tilde{y}_s - \tilde{y}| \sim (t_s - t)^{1/2}$. However, such a singularity is difficult to detect

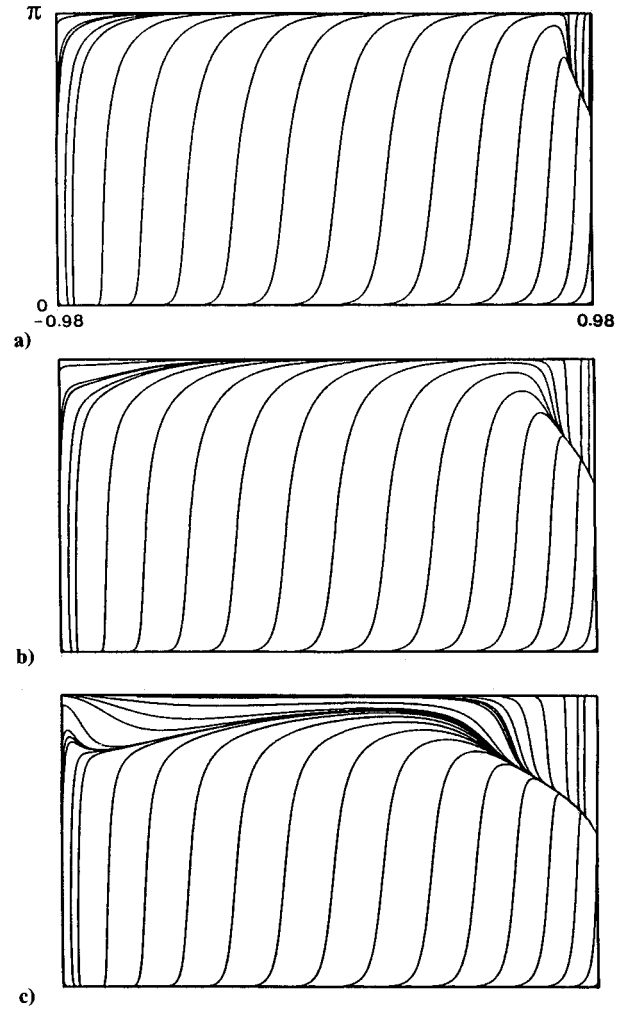

Fig. 10 Limiting streamlines in the main-body region ($\hat{\alpha} = 50$ deg): a) $t = 0.06$; b) $t = 0.08$; c) $t = 0.11$.

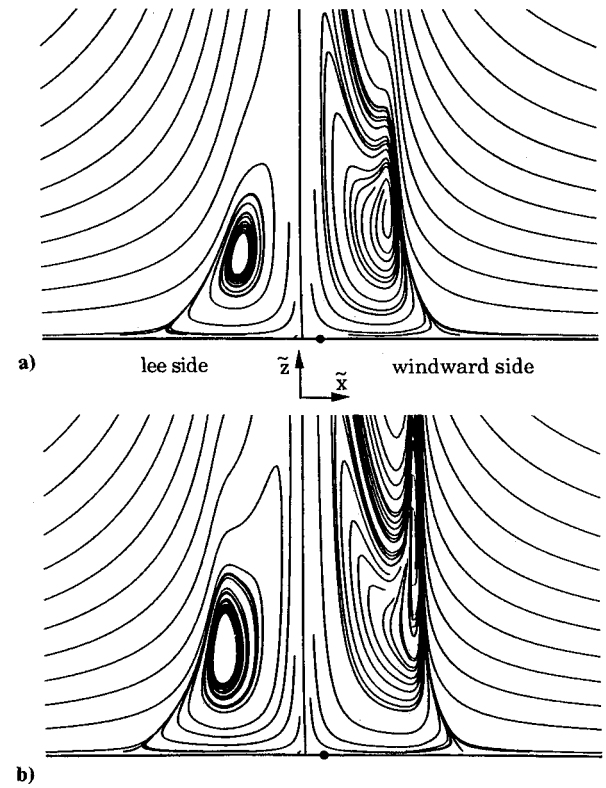

Fig. 11 Instantaneous streamlines in the symmetry plane of tail region ($\hat{\alpha} = 6$ deg): a) $t = 0.19$; b) $t = 0.21$.

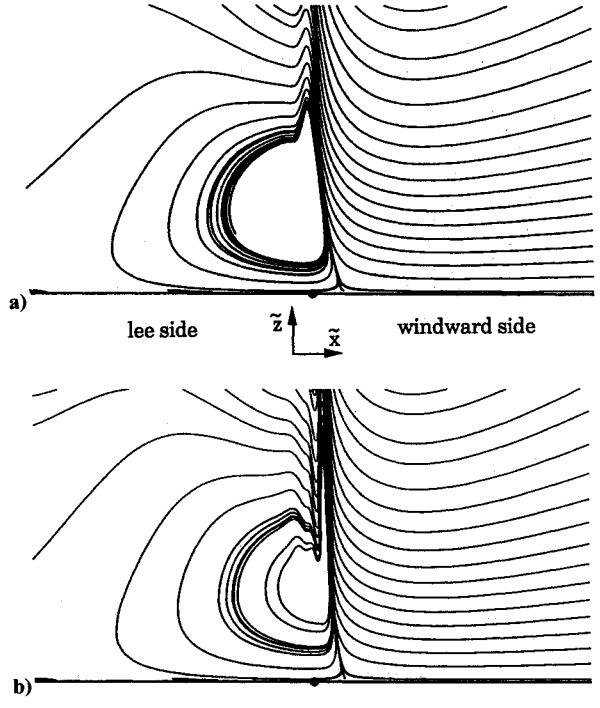

Fig. 12 Instantaneous streamlines in the symmetry plane of tail region ($\hat{\alpha} = 50$ deg): a) $t = 0.11$; b) $t = 0.12$.

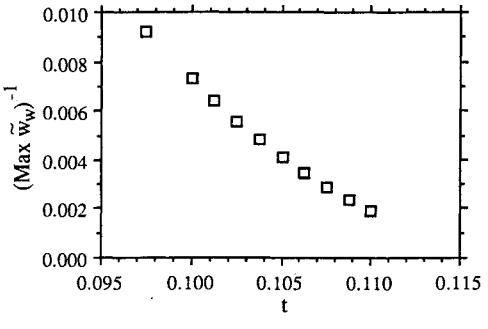

Fig. 13 Inverse of max $\tilde{w}_w$ vs t.

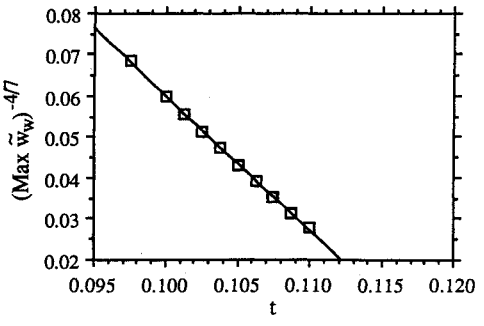

Fig. 14 (max $\tilde{w}_w$)$^{-4/7}$ vs t.

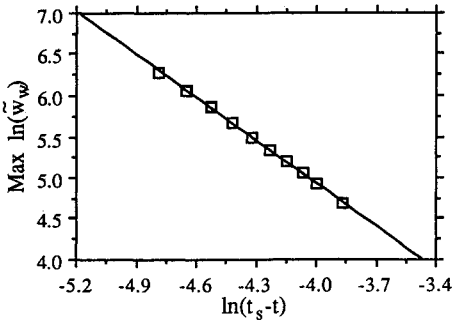

Fig. 15 Max $\ell n(\tilde{w}_w)$ vs $\ell n(t_s - t)$.

because in the Eulerian formulation the transverse coordinate $\tilde{z}$ is one of the independent variables. As suggested by Cowley,[3] the displacement velocity $\tilde{w}_w$ is expected to grow more rapidly than the displacement thickness when separation draws near. Consequently, $\tilde{w}_w$ serves as a good indicator of the presence of any singularity. In fact, from the definition of the displacement velocity [Eq. (11)] and using the aforementioned scaling as a guide, it is found that, to leading order approximation, the displacement velocity exhibits a much stronger singularity $(t_s - t)^{-7/4}$ at separation.

Quantitatively, the maximum value of $\tilde{w}_w$ obtained from the present computation is plotted against time t in Fig.13 for $\hat{\alpha} = 50$ deg. Because of the resolution problem, a singularity can, strictly speaking, never be truly identified from Eulerian numerical calculations. However, the tendency toward the formation of a singularity can be justified by the following assessment.

Assuming that near t_s the maximum $\tilde{w}_w$ does grow according to $(t_s - t)^{-7/4}$, then (max $\tilde{w}_w)^{-4/7}$ should approach zero linearly in $(t_s - t)$. The variation of (max $\tilde{w}_w)^{-4/7}$ with time t is shown in Fig. 14. The correlation coefficient (R^2) of the linear fitting is 0.999 in this case, indicating that the data do collapse onto a straight line. Linear extrapolation of the result estimates the separation time t_s to be 0.118. Using this t_s, the maximum value of $\ell n(\tilde{w}_w)$ is plotted as a function of $\ell n(t_s - t)$ in Fig. 15. Least-squares fitting of the data with a linear model shows that the straight line has a slope of -1.745, which is in good agreement with the analytical prediction ($-7/4$). The present numerical result thus lends support to the asymptotic theory of the singularity as described by van Dommelen and Cowley.[8]

Concluding Remarks

Unsteady boundary-layer separation has been controversial for some time. Increasing studies on this subject have led to a better understanding about the mechanism that initiates separation. Physically, separation in both the steady and unsteady cases has been identified to be resulting from the extreme streamwise contraction of a certain fluid packet inside the boundary layer, thus forcing the fluid above it to be ejected into the main stream. Traditional analyses focusing on the wall shear and limiting streamlines, although valuable for the steady problem, are not strictly applicable for the unsteady case.

The unsteady three-dimensional boundary-layer equations have been solved in the literature mostly by a marching procedure adapted from that developed for the steady boundary layer, and naturally some difficulties arise. In this paper it is properly posed as an initial-value problem in the Eulerian coordinates. The solution technique uses a factorization scheme with predictor-corrector formulation plus a multizone approach. Calculations have been carried out for an impulsively started prolate spheroid of axes ratio of ¼ at 6 and 50 deg incidences. In both cases separation is seen to initiate as a strong bursting of the boundary layer in the form of a narrow plume ejecting itself to the outer flow. Close to separation, the lateral distribution of the displacement velocity widens into a crescent shaped ridge predicted by van Dommelen and Cowley.[8] The instantaneous streamline pattern in the symmetry plane reveals the anatomy of the sharp spike signature near separation. The evolution of limiting streamlines in the tail region shows both the open and closed types of convergence patterns noted by Wang,[11-15] but there seems to be no apparent correlation with the initiation of the bursting at unsteady separation. Results from a linear regression analysis of the behavior of displacement velocity $\tilde{w}_w$ support the structure of the singularity at separation as derived from the Lagrangian theory of van Dommelen and Cowley.[8]

The present Eulerian scheme produces results that can be interpreted according to the Lagrangian concept of separation. In applications, it also enables us to look into questions of if and how the three-dimensional separation is generated and therefore how it may be influenced. Since an abrupt explosion in the displacement velocity characterizes separation, simulation may be attempted to control and alter its growth, e.g., by specifying different wall conditions to simulate the actions of actual moving surface or blowing/suction devices. In principle, the consequences of changing the parameters of a programmed distributed blowing or suction along the surface can be readily calculated. Thus, a gateway is open for further optimization.

Acknowledgment

The numerical calculation in this work was performed at the Cornell National Supercomputer Facility, a resource of the Center for Theory and Simulation in Science and Engineering.

References

[1]Van Dommelen, L. L., and Shen, S.-F., "The Spontaneous Generation of the Singularity in a Separating Laminar Boundary Layer," *Journal of Computational Physics,* Vol. 38, No. 2, 1980, pp. 125–140.

[2]Van Dommelen, L. L., "Unsteady Boundary-Layer Separation," Ph.D. Dissertation, Dept. of Mechanical Engineering, Cornell Univ., Ithaca, NY, May 1981.

[3]Cowley, S. J., "Computer Extension and Analytic Continuation of Blasius' Expansion for Impulsively Flow Past a Circular Cylinder," *Journal of Fluid Mechanics,* Vol. 135, Oct. 1983, pp. 389–405.

[4]Ingham, D. B., "Unsteady Separation," *Journal of Computational Physics,* Vol. 53, No. 1, 1984, pp. 90–99.

[5]Wu, T., and Shen, S.-F., "A Multi-Zone Time-Marching Technique for Unsteady Separating Three-Dimensional Boundary Layer and its Application to the Symmetry-Plane Solution of an Impulsively-Started Prolate Spheroid," *Journal of Fluids Engineering,* Vol. 113, June 1991, pp. 228–239.

[6]Shen, S.-F., and Wu, T., "Unsteady Separation over Maneuvering Bodies," *AIAA Journal,* Vol. 28, No. 12, 1990, pp. 2059–2068.

[7]Shen, S.-F., "Unsteady Separation of Three-Dimensional Boundary Layers from the Lagrangian Viewpoint," *Nonsteady Fluid Dynamics,* edited by D. E. Crow and J. A. Miller, American Society of Mechanical Engineers, New York, Dec. 1978, pp. 47–51.

[8]Van Dommelen, L. L., and Cowley, S. J., "On the Lagrangian Description of Unsteady Boundary-Layer Separation. Part I : General Theory," *Journal of Fluid Mechanics,* Vol. 210, Jan. 1990, pp. 593–626.

[9]Xu, W. C., and Wang, K. C., "Unsteady Laminar Boundary Layer Along the Symmetry Plane of an Impulsively Started Prolate Spheroid," *Journal of Fluid Mechanics,* Vol. 195, Oct. 1988, pp. 413–435.

[10]Werle, H., "Separation on Axisymmetrical Bodies at Low Speed," *La Recherche Aeronautique,* Vol. 90, Sept. 1962, pp. 3–14.

[11]Wang, K. C., "Separation Patterns of Boundary Layer over an Inclined Body of Revolution," *AIAA Journal,* Vol. 10, No. 8, 1972, pp. 1044–1050.

[12]Wang, K. C., "Laminar Boundary Layer Over a Body of Revolution at Extremely High Incidence," *Physics of Fluids,* Vol. 17, No. 7, 1974, pp. 1381–1385.

[13]Wang, K. C., "Boundary Layer Over a Blunt Body at High Incidence with an Open-Type of Separation," *Proceedings of the Royal Society of London,* Series A, Vol. 340, No. 1620, 1974, pp. 33–55.

[14]Wang, K. C., "Laminar Boundary Layer near the Symmetry Plane of a Prolate Spheroid," *AIAA Journal,* Vol. 12, No. 7, 1974, pp. 949–958.

[15]Wang, K. C., "Boundary Layer Over a Blunt Body at Low Incidence with Circumferential Reversed Flow," *Journal of Fluid Mechanics,* Vol, 72, Nov. 1975, pp. 49–65.

[16]Cebeci, T., Khattab, A. A., and Stewartson, K., "Three-Dimensional Laminar Boundary Layers and OK of Accessibility," *Journal of Fluid Mechanics,* Vol. 107, June 1981, pp. 57–87.

[17]Cebeci, T., and Su, W., "Separation of Three-Dimensional Laminar Boundary Layers on a Prolate Spheroid," *Journal of Fluid Mechanics,* Vol. 191, June 1988, pp. 47–77.

[18]Vatsa, V. N., Thomas, J. L., and Wedan, B. W., "Navier-Stokes Computations of a Prolate Spheroid at Angle of Attack," *Journal of Aircraft,* Vol. 26, No. 11, 1989, pp. 986–993.

[19]Ragab, S. A., "A Method for the Calculation of Three-Dimensional Boundary Layers with Circumferential Reversed Flow on Bodies," AIAA Paper 82-1023, June 1982.

[20]Ragab, S. A., "The Laminar Boundary Layer on a Prolate Spheroid Started Impulsively from Rest at High Incidence," AIAA Paper 86-1109, May 1986.

[21]Cebeci, T., Khattab, A. A., and Stewartson, K., "On Nose Separation," *Journal of Fluid Mechanics,* Vol. 97, April 1980, pp. 435–454.

[22]Wu, T., "Numerical Studies of Unsteady Laminar Boundary-Layer Separation over Impulsively-Started Moving Objects," Ph.D. Dissertation, Cornell Univ., Dept. of Mechanical Engineering, Ithaca, NY, Aug. 1991.

[23]Wang, K. C., "On the Determination of the Zones of Influence and Dependence for Three-Dimensional Boundary-Layer Equations," *Journal of Fluid Mechanics,* Vol. 48, July 1971, pp. 397–404.

[24]Douglas, J., and Jones, B. F., "On Predictor-Corrector Methods for Non Linear Parabolic Differential Equations," *Journal of Society for Industrial and Applied Mathematics,* Vol. 11, No. 1, 1963, pp. 195–204.

[25]Warming, R. F., and Beam, R. M., "On the Construction and Application of Implicit Factored Schemes for Conservation Laws," *Proceedings of the Symposium in Applied Mathematics of the American Mathematical Society and the Society for Industrial and Applied Mathematics,* edited by H. B. Keller, American Mathematical Society, New York, April 1977, pp. 85–125.

[26]Howarth, L., "The Boundary Layer in Three Dimensional Flow—Part 2. The Flow Near a Stagnation Point," *Philosophical Magazine,* Series 7, Vol. 42, No. 335, 1951, pp. 1433–1440.

[27]Moore, F. K., "Displacement Effect of a Three-Dimensional Boundary Layer," NACA Rept. 1124, Aug. 1953.

[28]Lighthill, M. J., "Boundary Layer Theory," *Laminar Boundary Layers,* 1st ed., edited by L. Rosenhead, Oxford Univ. Press, London, 1963, pp. 78–80.

[29]Chapman, G. T., "Topological Classification of Flow Separation on Three-Dimensional Bodies," AIAA Paper 86-0485, Jan. 1986.

[30]Cebeci, T., and Su, W., "Birth of Open Separation on a Prolate Spheroid," Air Force Office of Scientific Research, AFOSR-TR-88-1178, Washington, DC, Sept. 1988.